Journal of Science and Transport Technology

University of Transport Technology

Application of an artificial neural network and QCM sensor coated with γ-Fe_2O_3 nanoparticles for estimation of SO_2 gas sensing characteristics

Nguyen Thanh Vinh[1,2], Tran Quoc Tuan[1], Nguyen Van Cuong[1], Cao Xuan Truong[2], Nguyen Van Quy[2*]

[1]University of Transport Technology, No.54 Trieu Khuc, Thanh Xuan District, Ha Noi 100000, Viet Nam

[2]International Training Institute for Materials Science, Ha Noi University of Science and Technology, No. 1 Dai Co Viet, Hai Ba Trung District, Ha Noi 100000, Viet Nam

Article info

Type of article:
Original research paper

***Corresponding author:**
E-mail address:
quy.nguyenvan@hust.edu.vn

Received:
December 11, 2021
Accepted:
March 01, 2022
Published:
March 14, 2022

Abstract: γ-Fe_2O_3 nanoparticles (NPs) were synthesized by co-precipitation method and a following annealing treatment at 200 °C in ambient air for 6 hours. A mass-type sensor was prepared by coating γ-Fe_2O_3 NPs on the active electrode of quartz crystal microbalance (QCM). The obtained results of the γ-Fe_2O_3 NPs based QCM sensor indicate the high response and good repeatability toward SO_2 gas in the range of 2.5 – 20 ppm at room temperature. Moreover, the frequency shift (ΔF) and change in mass of SO_2 adsorption per unit area (Δm) of the γ-Fe_2O_3 NPs coated QCM sensor have a relationship with the mass density of γ-Fe_2O_3 NPs and SO_2 concentrations. The artificial neural network (ANN) model using Levenberg-Marquardt optimization was used to handle the ΔF and Δm of the γ-Fe_2O_3 NPs coated QCM sensor. The results of the model validation proved to be a reliable way between the experiment and prediction values.

Keywords: QCM, SO_2, γ-Fe_2O_3, gas sensor, ANN

1. Introduction

Nowadays, the development of modern society has created many sources of pollution emission. One of the major global concerns is air pollution which puts pressure on governments or countries as well as, negative effects on health and quality of human daily life [1], [2], [3]. Among them, sulfur dioxide (SO_2) is always in the top toxic gases causing respiratory diseases, bronchoconstriction and dyspnea [2], [4], [5]. Therefore, air quality guidelines are developed and continuously updated by the World Health Organization (WHO). The current standard of air quality is 20 μg/m^3 (8 ppb) and 500 μg/m^3 (190 ppb) when people expose to SO_2 for 24 hours and 10 minutes, respectively [6]. The immediate danger to life and health (IDLH) values and the short-term exposure limit (TLV-STEL) of SO_2 according to ACGIH are 100 and 5 ppm, respectively [7]. However, according to P.D. Hien's report on the air pollution level of the urban districts of Ha Noi, Viet Nam in 2020, the SO_2 concentrations reached the highest point of 35 μg/m^3 in Hoan Kiem, while Thanh Xuan was 22.5 (μg/m^3) [8]. These pollution levels were higher than those recommended by WHO. Accordingly, SO_2 sensors must be seriously

considered and developed. These works could contribute to environmental pollution monitoring and ensuring social guarantee.

Currently, there are many types of SO_2 sensors that have been successfully developed with different operation principles [9], [10], [11], [12]. Among them, the mass-type sensor using quartz crystal microbalance (QCM) is highly appreciated for its low power consumption, good response (nanogram level) and stable operation at room temperature [13], [14]. QCM sensors coated with iron oxide show excellent detection performance to SO_2 gas [15]–[17], and γ-Fe_2O_3 is an outstanding sensing material [18], [19]. So far, numerous researches have been published for the purpose of protease, alcohol and gas classification using QCM sensors, which were supported by machine learning [20]–[23], [24]. The positive results show the considerable application potential of this field. However, machine learning is less common in SO_2 detection studies of QCM sensors in general and QCM coated with γ-Fe_2O_3 in particular. Therefore, in this work, the SO_2 sensor was made from γ-Fe_2O_3 nanoparticles (NPs) coated on the gold electrode of QCM. The basic characteristics of sensor were investigated, and these experimental data were used for a machine learning. The built algorithm was used to predict the output signals of QCM sensor (frequency shift/ΔF, and the mass change of adsorption SO_2 per unit area of sensing material/Δm), these predictions agree with the experimental results after the training process.

2. Experiment

2.1. γ-Fe_2O_3 NPs synthesis

The chemicals used in this experiment were ferric chloride hexahydrate ($FeCl_3.6H_2O$, > 98%), ferrous chloride tetrahydrate ($FeCl_2.4H_2O$, > 98%) and sodium hydroxide (NaOH, >98%). These chemicals were purchased from Xilong Scientific Co., Ltd. (Guang-dong, China).

In this work, γ-Fe_2O_3 NPs were synthesized through co-precipitation, followed by annealing treatment. The detail of synthesis process was described in our previous publication [19]. In brief, the precursors of $FeCl_3.6H_2O$ (0,05 mol) and $FeCl_2.4H_2O$ (0,025 mol) were dissolved in deionized water (DI). 2M NaOH was then added to this mixed solution at 80 °C. The precipitate was dried and calcined at 200 °C in ambient air for 6 hours to obtain γ-Fe_2O_3 NPs. The as-prepared γ-Fe_2O_3 NPs was dissolved and deposited on the electrode of QCM by using spray-coating method [17]. γ-Fe_2O_3 NPs were crushed and dispersed in DI with a concentration of 1 mg ml^{-1}. In order to fabricate a QCM sensor, 3 ml of dispersed solution was used for each experiment at the flow rate of 0.2 ml min^{-1}. SO_2 sensing characteristics of QCM sensor were performed with the change in γ-Fe_2O_3 NPs layer. The number of sensing material layers, γ-Fe_2O_3 NPs mass density deposited on the electrode (m_γ-Fe_2O_3) and the resonance frequency of QCM (F-resonance) corresponding to each layer are shown in Table. 1.

Table. 1. The parameters of QCM sensor was fabricated

No.	Layer	F-resonance (Hz)	m_γ-Fe_2O_3 (μg.cm^{-2})
	uncoated	5001725.8	0
1	1st	4995656.1	107.24
2	2nd	4989780.1	211.05
3	3rd	4983067.6	329.65
4	4th	4978063.8	418.06
5	5th	4973373.8	500.92
6	6th	4967813.1	599.16
7	7th	4962879.0	686.34

The gas sensor properties were investigated with SO_2 gas through a home-made measurement system and QCM200 digital controller linked to PC by using SRSQCM200 software program [25], [26]. XRD pattern of γ-Fe_2O_3 was recorded in the range of 2θ: 20 – 70° using Cu Kα radiation with λ of 0.1542 nm. The morphology of iron oxide was observed by S-4800 Scanning Electron Microscopy device (Hitachi).

2.2. Machine learning for estimation of QCM frequency shift and the mass change of adsorption SO_2 per unit area

2.2.1. Artificial Neural Network

Artificial Neural Network (ANN) is an useful algorithm for solving prediction and classification problems [27], [28]. In this work, the experimental data were used for the development of an ANN model. The Levenberg-Marquardt algorithm was considered the most suitable for ANN with a training dataset [28], [29]. Therefore, ANN based on the Levenberg-Marquardt algorithm was used in this study to optimize the searching process for neurons weights and biases.

2.2.2. Cross-fold validation

Cross-validation (CV) is a popular technique to evaluate a model more fully and accurately for the moderate-sized training in the field of machine learning. In k-Fold cross-validation (k-Fold CV), the training dataset is randomly split into subsets of approximately equal size (k is an integer). The machine is trained k times in which one random subset is selected as the validation data, the other subsets (k-1) are selected as the training data for each time. The cross-validation estimate of accuracy results from the average evaluation of all runs [30]. In this work, k = 10 was chosen to split the training dataset due to minor errors and low variances through experimentation [31]. On the other hand, the test dataset checks the model's response in the final step when dealing with unseen data.

2.2.3. Model evaluation

In this paper, the coefficient of determination (R^2) and the root of the mean square error (RMSE) are used to evaluate the accuracy of the machine learning model in predicting Δm and ΔF. Precisely, R^2 shows the square correlation between the predicted value and the actual value, RMSE index calculates the average of the square of the difference between the predicted value and the actual value. These values are determined by equations (1) [32] and (2) [33]:

$$\mathrm{RMSE} = \sqrt{\frac{1}{n}\sum_{i=1}^{m}\left(e_i - m_i\right)^2} \quad (1)$$

$$R^2 = \frac{\sum_{i=1}^{m}\left(e_i - \bar{e}\right)\left(m_i - \bar{m}\right)}{\sqrt{\sum_{i=1}^{m}\left(e_i - \bar{e}\right)^2 \sum_{i=1}^{m}\left(m_i - \bar{m}\right)^2}} \quad (2)$$

Where e_i is the estimated value and m_i is the measured value; $\bar{e}$ and $\bar{m}$ are the average of estimated value and measured value, respectively.

3. Results and discussion

3.1. The crystalline structure and morphological of as-prepared sample

Fig. 1 shows the morphological and structural characteristics of γ-Fe_2O_3 material via XRD and SEM results. The XRD pattern of the as-prepared sample is indicated in Fig. 1a. The strong diffraction peaks at about 30.3°, 35.4°, 43.2°, 53.4°, 57.1°, and 62.6° are well-matched with the (220), (311), (400), (422), (511) and (440) lattice planes, respectively. In comparison with the standard cards (JCPDS No. 19 – 0629 and No. 39.1346), it is clearly seen that the as-prepared iron oxide material is either Fe_3O_4 or γ-Fe_2O_3. However, Fe_3O_4 material was transferred to γ-Fe_2O_3 at 200 °C due to magnetite oxidation and their similar to crystal structures [18], [34], [35], [36]. Thus, the crystallite of the synthesized iron oxide in this work indicates a crystal structure of γ-Fe_2O_3. Fig. 1b shows SEM image of the as-prepared γ-Fe_2O_3. The morphology of γ-Fe_2O_3 exhibits a spherical appearance. Although the nanoparticles were slightly agglomerated, the particles individually expose with diameter of 50 nm. In consequence, γ-Fe_2O_3 NPs were successfully synthesized by co-precipitation and following calcining in air. Moreover, the mini image of QCM sensor coated with γ-Fe_2O_3 NPs is shown in the insert of the Fig. 1b. As observed in the mini image, the γ-Fe_2O_3 NPs fully covered the electrode.

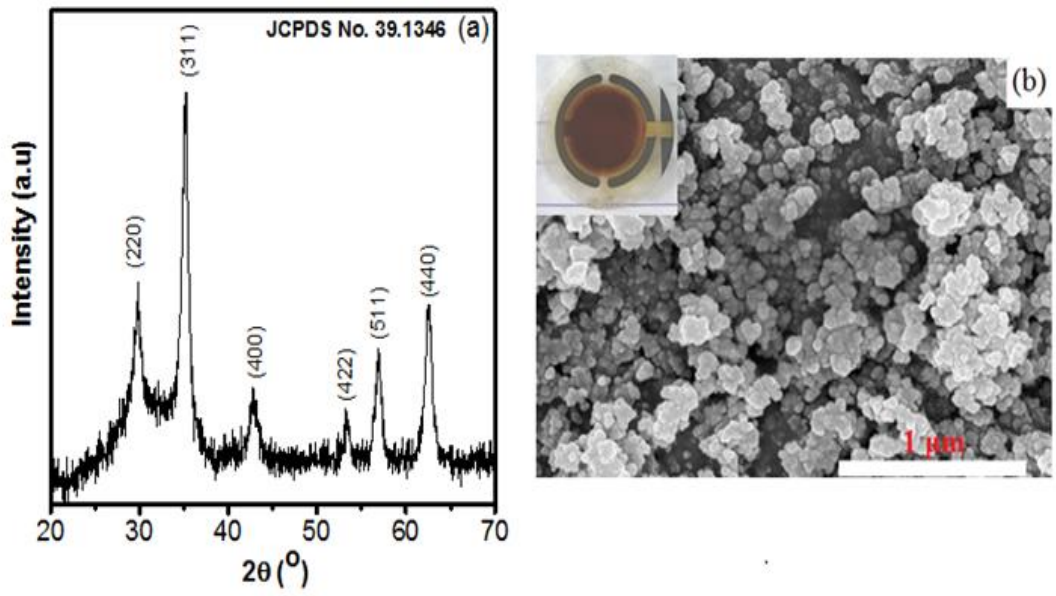

Fig. 1. (a) XRD, (b) SEM of γ-Fe_2O_3 NPs and image of QCM sensor coated with γ-Fe_2O_3 NPs

3.2. Experiment results

The response – recovery curves of QCM sensor with the 1st layer of sensing material towards SO_2 concentration range of 2.5 – 20 ppm are described in Fig. 2. The SO_2 molecules are adsorbed on sensing materials of γ-Fe_2O_3 NPs via hydrogen bonding and like-hydrogen bonds [18], [19]. Fig. 2a shows the change in mass of SO_2 adsorption per unit area for each on/off cycle of the target gas. It is clear that the Δm increases with increasing SO_2 concentration. Namely, the adsorptions of SO_2 are 0.004, 0.010, 0.028, 0.047, and 0.065 μg.cm^{-2} at 2.5, 5, 10, 15, and 20 ppm of SO_2 concentrations, respectively. The relationship between Δm and the ΔF of QCM can be determined by Suaerbrey's equation [37]

$$\Delta F = - C_f.\Delta m \quad (3)$$

Where ΔF is in Hertz (Hz), Δm is in μg cm^{-2} and C_f is the sensitivity factor in Hz μg^{-1} cm^2 (C_f = 56.6 Hz μg^{-1} cm^2 for a 5 MHz AT-cut QCM).

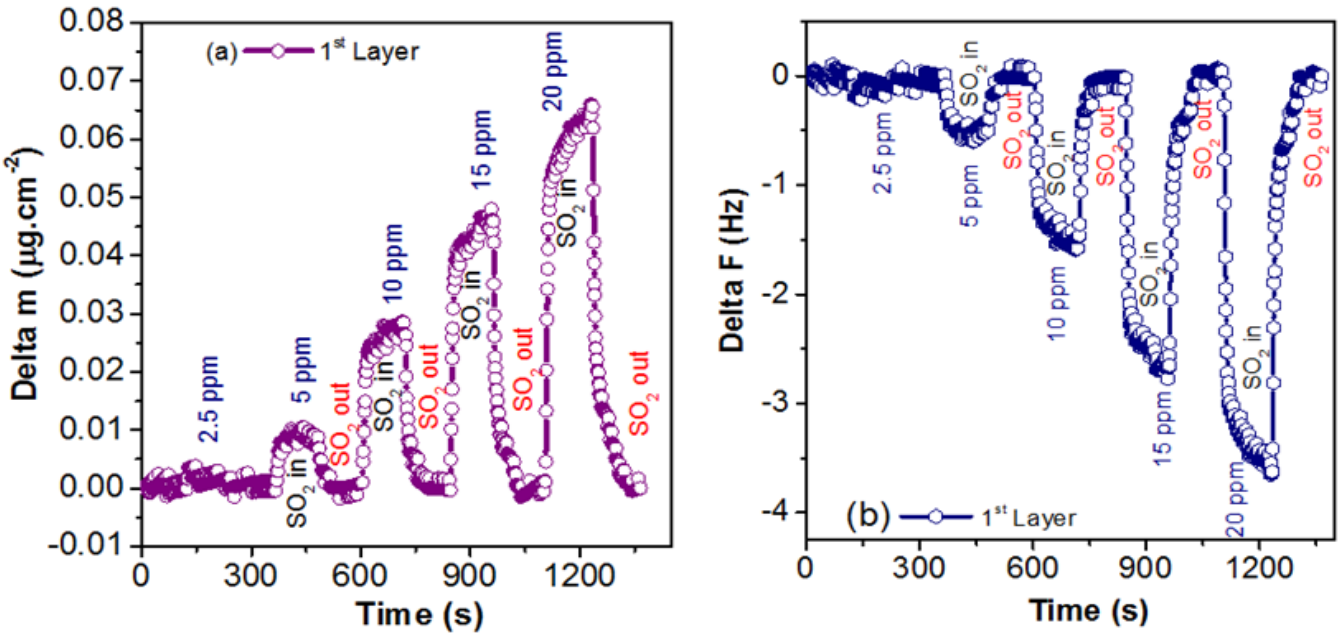

Fig. 2. The response – recovery curves of QCM sensor coated with γ-Fe_2O_3: (a) Δm, (b) ΔF

Based on equation (3), the resonance frequency of QCM will reduce when SO_2 mass adsorbed on the electrode increases. Similarly, the change in frequency versus time of the sensor towards different SO_2 concentrations is shown in Fig. 2b. The maximum frequency shifts of the QCM sensor towards 2.5, 5, 10, 15 and 20 were about 0.23, 0.69, 1.68, 2.77, and 3.74 Hz, respectively. Thus, the QCM sensor coated with γ-Fe_2O_3 NPs indicated the excellent response to low SO_2 concentrations at room temperature. Fig. 3 shows the repeatability of the sensor for four cycles at 10 and 15 ppm in real-time. The characteristics of frequency shift – time curve are similar for all cycles at the same concentration. The results indicate that the γ-Fe_2O_3 NPs sensor has good repeatability for SO_2 gas. Fig. 4 describes the response signals of sensor at different SO_2 concentrations. The responses not only depend on SO_2 concentration but also the mass density of γ-Fe_2O_3 NPs layer deposited on the electrode of QCM. It is obvious that the increase in ΔF is visibly proportional to the target gas concentration and mass density of the sensing material.

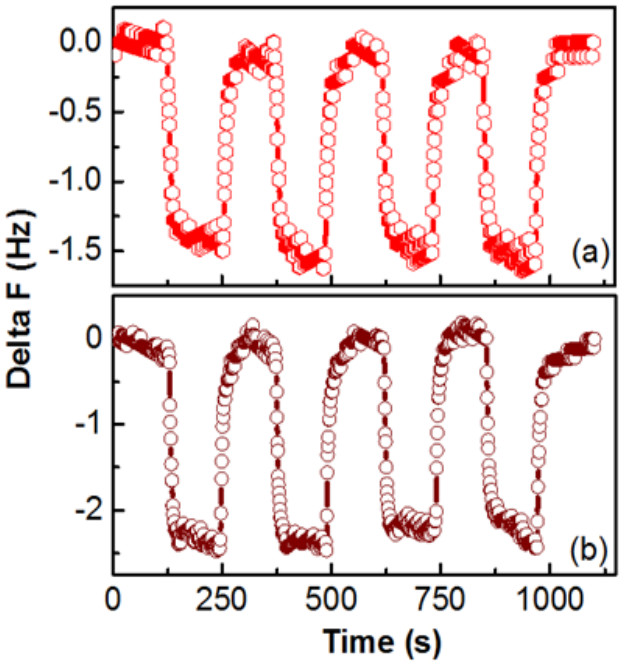

Fig. 3. The repeatability of QCM sensor coated with γ-Fe_2O_3 at (a) 10 and (b) 15 ppm of SO_2 concentration

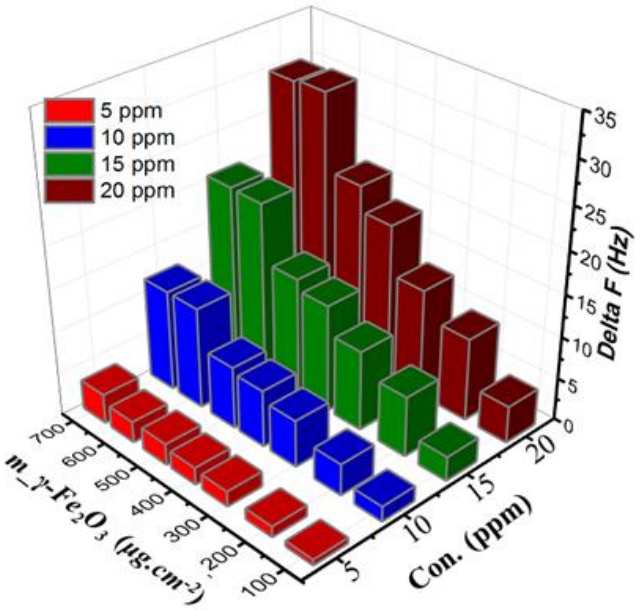

Fig. 4. The frequency shifts of QCM sensor depend on SO_2 concentration and m_γ-Fe_2O_3 NPs deposited on the QCM electrode

3.3. Simulation results

This paper develops an ANN model (with the 3-4-1 architecture) based on experimental data of SO_2 gas sensing properties. The sensing material layer, m_γ-Fe_2O_3 and SO_2 concentration are input variables, whereas Δm and ΔF are output variables. Fig. 5 shows the distribution and the correlation of the parameters in this study. In addition, Fig. 5 also indicates the correlation of input variables, input and output variables, and output variables. Based on the value of the Pearson correlation coefficient (R), it can be seen that the layer and m_γ-Fe_2O_3 have a considerable correlation (R = 1), so they are dependent variables; concentration and m_γ-Fe_2O_3, layer are independent variables, these correlations are weak (R = 0.01 and 0.02, respectively). Moreover, the correlation between input variables (layer, m_γ-Fe_2O_3) and output variables (Δm, ΔF) are moderate (R = 0.52) while SO_2 concentration has a significant correlation with both Δm and ΔF. Especially, the output variables' (Δm&ΔF) correlation is considerable (R = 1). Based on the analysis of simulation results, Con. of SO_2 and m_γ-Fe_2O_3 of the data set could increase the accuracy and generality of the prediction model.

The building process of the ANN model is carried out in two stages for 110 experiment samples: (i) the training phase, 10-Fold CV was used during the training phase of the ANN model with 70% dataset; (ii) the testing phase, when ANN model tool achieves the optimal prediction performance, 30% other of the dataset was used to evaluate the predictive performance of ANN on unseen data. The results of the ANN model prediction performance evaluation for output variables are shown in Fig. 6. Ten different simulations were carried out, denoted from CV-1 to CV-10. It is clear that ANN model using Levenberg-Marquardt optimization has very good predictive capability. Namely, CV-2 of ΔF and CV-4 of Δm could be considered the typical model prediction. The R^2 is the highest while RMSE is the lowest for the test dataset. Thus, the typical prediction results of the ANN model are presented via regression graphs as shown in Fig. 7. The regression model shows the correlation between predicted ΔF, Δm according to the ANN model and actual values from the experiments for the training dataset (Fig. 7a, c) and the testing dataset (Fig. 7b, d), respectively. The suggested values from the AI model for the training, testing dataset and the values obtained from the experiment are very closely distributed on the diagonal. The performance of this ANN model is evaluated by the statistical index, such as: RMSE and R^2. Additionally, the best ΔF, Δm prediction results of RMSE and R^2 are 0.4229, 0.007836 and 0.9964, 0.9963 for the training dataset, and these are 0.5492, 0.008226 and 0.9933, 0.9942 for the testing dataset, respectively. The high values of R^2 and low RMSE of the proposed ANN model indicated the ability to predict accurately and the excellent generalization performance in predicting the outputs.

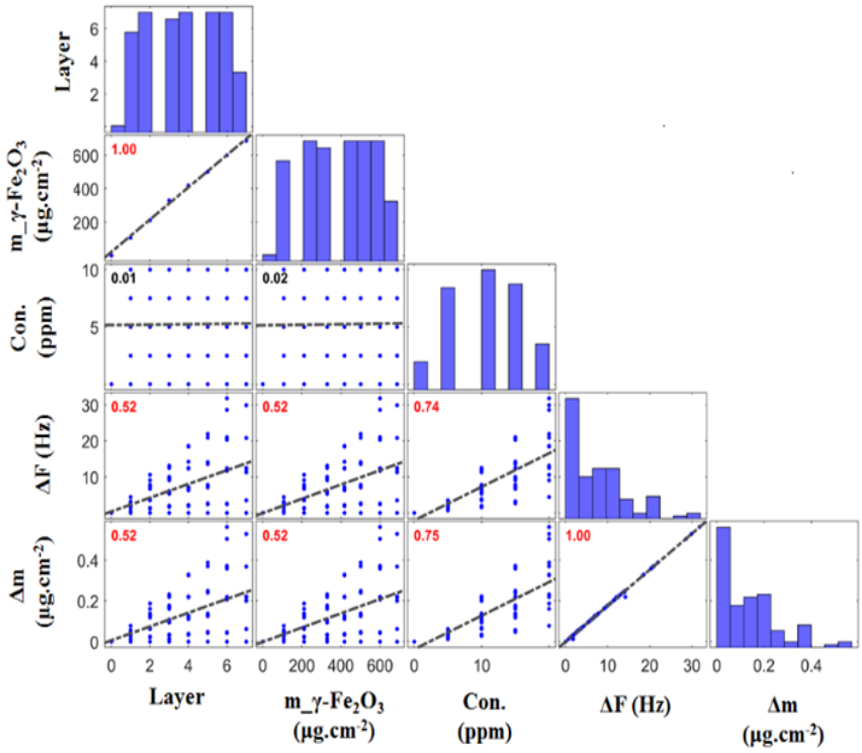

Fig. 5. Histogram and correlation analysis between input and output parameters considered in this study

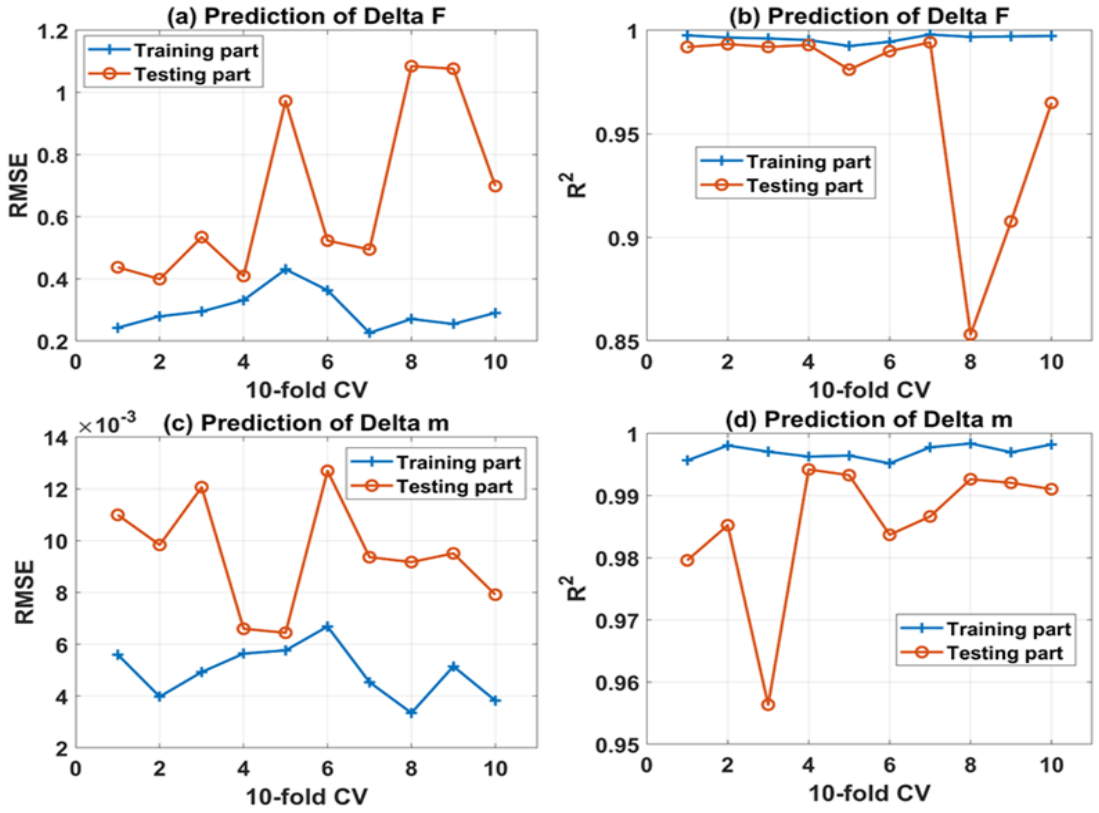

Fig. 6. The results of training and validation of (a b) ΔF and (c, d) Δm

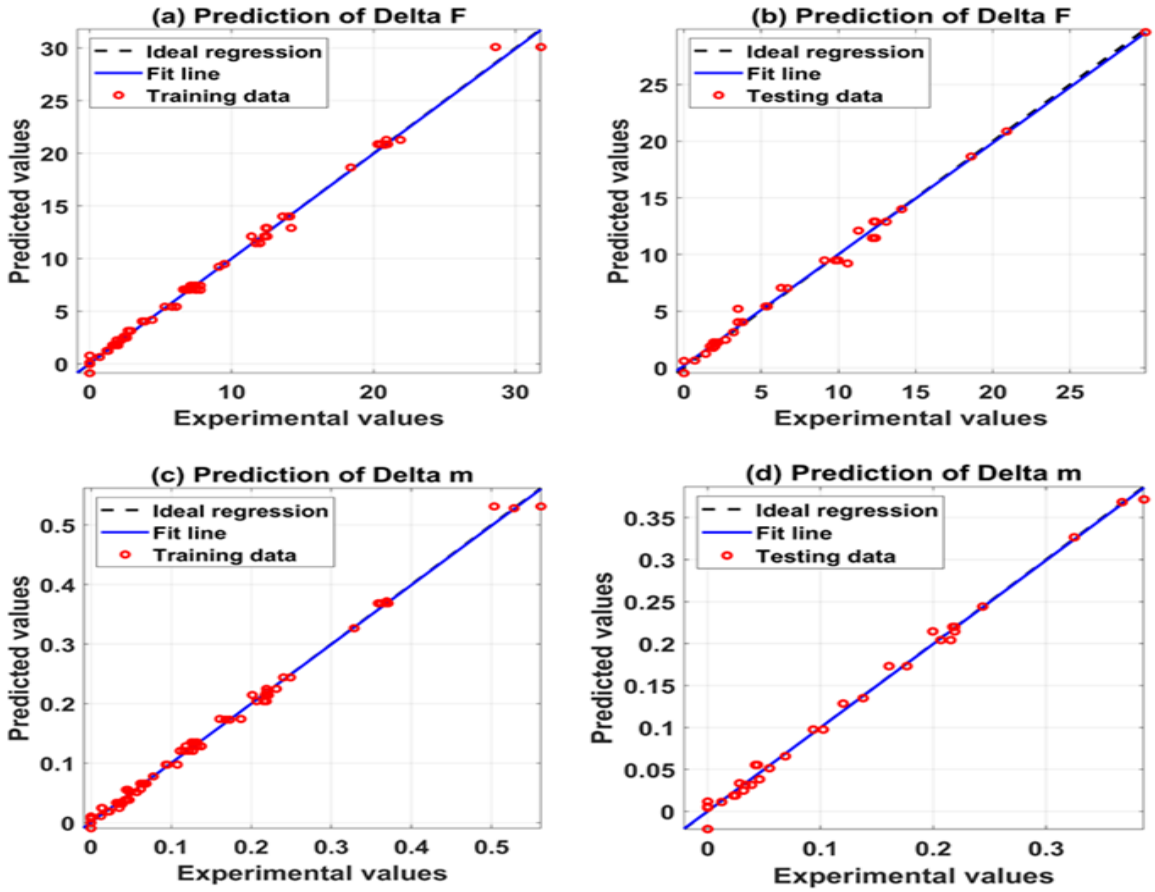

Fig. 7. The estimated values versus true values for (a) training and (b) testing data of ΔF; (c) training and (d) testing data of Δm

4. Conclusion

A QCM sensor based on γ-Fe_2O_3 NPs as a sensing material was fabricated. The sensor exposed high response, good repeatability towards low concentration of SO_2 at room temperature. The SO_2 gas response of the QCM sensor increases with increasing target gas concentration and mass density of γ-Fe_2O_3. Furthermore, the ANN model using the Levenberg-Marquardt optimization proves the capable and accurate estimation of output (the frequency shift and the change in mass of adsorption SO_2 per unit area) versus input variables (m_γ-Fe_2O_3 and SO_2 concentration) of QCM sensor. These results bring forward a potential application of machine learning in the field of QCM sensor in the near future.

Acknowledgments

This research is funded by University of Transport Technology (UTT) under grant number 2021-09-ĐTTĐUTT

References

[1] X.-C. Wang *et al.*, “Air pollution terrain nexus: A review considering energy generation and consumption,” *Renew. Sustain. Energy Rev.*, vol. 105, no. December 2018, pp. 71–85, May 2019, doi: 10.1016/j.rser.2019.01.049.

[2] L. W. Stanek and J. S. Brown, “Air Pollution: Sources, Regulation, and Health Effects,” in *Reference Module in Biomedical Sciences*, no. June, Elsevier, 2019, pp. 1–10.

[3] S. Rajagopalan, S. G. Al-Kindi, and R. D. Brook, “Air Pollution and Cardiovascular Disease,” *J. Am. Coll. Cardiol.*, vol. 72, no. 17, pp. 2054–2070, Oct. 2018, doi: 10.1016/j.jacc.2018.07.099.

[4] D. P. Rall, “Review of the health effects of sulfur oxides,” *Environ. Health Perspect.*, vol. Vol 8, no. August, pp. 97–121, 1974, doi: 10.2307/3428194.

[5] P. R. Arghya Sardar, “SO_2 Emission Control and Finding a Way Out to Produce Sulphuric Acid from Industrial SO_2 Emission,” *J. Chem. Eng. Process Technol.*, vol. 06, no. 02, 2015, doi: 10.4172/2157-7048.1000230.

[6] M. Krzyzanowski and A. Cohen, “Update of WHO air quality guidelines,” *Air Qual. Atmos. Heal.*, vol. 1, no. 1, pp. 7–13, 2008, doi: 10.1007/s11869-008-0008-9.

[7] National Institute for Occupational Safety and Health, “Threshold Limit Values (TLV) and Immediately Dangerous to Life and Health (IDLH) values,” *Saf. Heal.*, p. 1, 2005.

[8] P. D. Hien, N. T. Men, P. M. Tan, and M. Hangartner, “Impact of urban expansion on the air pollution landscape: A case study of Hanoi, Vietnam,” *Sci. Total Environ.*, vol. 702, p. 134635, Feb. 2020, doi: 10.1016/j.scitotenv.2019.134635.

[9] P. Tyagi, A. Sharma, M. Tomar, and V. Gupta, *Metal oxide catalyst assisted SnO_2 thin film based SO_2 gas sensor*, vol. 224. Elsevier B.V., 2016.

[10] M. Barzegar Gerdroodbary, D. D. Ganji, I. Shiryanpour, and R. Moradi, “Mass analysis of CH_4/SO_2 gas mixture by low-pressure MEMS gas sensor,” *J. Nat. Gas Sci. Eng.*, vol. 53, pp. 317–328, 2018, doi: 10.1016/j.jngse.2018.03.002.

[11] N. D. Hoang, V. Van Cat, M. H. Nam, V. N. Phan, L. A. Tuan, and N. Van Quy, “Enhanced SO_2 sensing characteristics of multi-wall carbon nanotubes based mass-type sensor using two-step purification process,” *Sensors Actuators A Phys.*, vol. 295, pp. 696–702, 2019, doi: 10.1016/j.sna.2019.06.046.

[12] Y. Tian, K. Qu, and X. Zeng, “Investigation into the ring-substituted polyanilines and their application for the detection and adsorption of sulfur dioxide,” *Sensors Actuators, B Chem.*, vol. 249, pp. 423–430, 2017, doi: 10.1016/j.snb.2017.04.057.

[13] A. Alassi, M. Benammar, and D. Brett, “Quartz crystal microbalance electronic interfacing systems: A review,” *Sensors (Switzerland)*, vol. 17, no. 12, pp. 1–41, 2017, doi: 10.3390/s17122799.

[14] N. L. Bragazzi, D. Amicizia, D. Panatto, D. Tramalloni, I. Valle, and R. Gasparini, *Quartz-Crystal Microbalance (QCM) for Public Health: An Overview of Its Applications*, 1st ed., vol. 101. Elsevier Inc., 2015.

[15] N. T. Vinh *et al.*, "Dual-functional sensing properties of $ZnFe_2O_4$ nanoparticles for detection of the chloramphenicol antibiotic and sulphur dioxide gas," *Sensors Actuators A Phys.*, vol. 332, p. 113093, Dec. 2021, doi: 10.1016/j.sna.2021.113093.

[16] N. V. Q. Nguyen Thanh Vinh, Vu Ngoc Phan, Man Hoai Nam, Le Anh Tuan, "NO_2 gas sensor based on QCM coated with iron oxide nanorods," *Vietnam J. Sci. Technol.*, vol. 58, no. 2, pp. 204–211, 2020, doi: 10.15625/2525-2518/58/2/14225.

[17] N. T. Vinh, L. A. Tuan, L. K. Vinh, and N. Van Quy, "Synthesis, characterization, and gas sensing properties of Fe_3O_4/FeOOH nanocomposites for a mass-type gas sensor," *Mater. Sci. Semicond. Process.*, vol. 118, no. April, p. 105211, Nov. 2020, doi: 10.1016/j.mssp.2020.105211.

[18] T. V. Nguyen *et al.*, "Effect of the phase composition of iron oxide nanorods on SO_2 gas sensing performance," *Mater. Res. Bull.*, vol. 134, no. September 2020, p. 111087, Feb. 2021, doi: 10.1016/j.materresbull.2020.111087.

[19] N. Thanh Vinh *et al.*, "Effect of ferric ion [$Fe3^+$] and [Fe^{2+}] on SO_2 adsorption ability of γ-Fe_2O_3 nanoparticles for mass-type gas sensors," *Sensors Actuators A Phys.*, vol. 331, no. 3, p. 112981, Nov. 2021, doi: 10.1016/j.sna.2021.112981.

[20] M. Tatarko *et al.*, "Machine learning enabled acoustic detection of sub-nanomolar concentration of trypsin and plasmin in solution," *Sensors Actuators, B Chem.*, vol. 272, pp. 282–288, 2018, doi: 10.1016/j.snb.2018.05.100.

[21] M. F. Adak, P. Lieberzeit, P. Jarujamrus, and N. Yumusak, "Classification of alcohols obtained by QCM sensors with different characteristics using ABC based neural network," *Eng. Sci. Technol. an Int. J.*, vol. 23, no. 3, pp. 463–469, 2020, doi: 10.1016/j.jestch.2019.06.011.

[22] E. Oleneva, T. Kuchmenko, E. Drozdova, A. Legin, and D. Kirsanov, "Identification of plastic toys contaminated with volatile organic compounds using QCM gas sensor array," *Talanta*, vol. 211, no. December 2019, p. 120701, 2020, doi: 10.1016/j.talanta.2019.120701.

[23] A. Özmen, F. Tekce, M. A. Ebeoğlu, C. Taşaltin, and Z. Z. Öztürk, "Finding the composition of gas mixtures by a phthalocyanine-coated QCM sensor array and an artificial neural network," *Sensors Actuators, B Chem.*, vol. 115, no. 1, pp. 450–454, 2006, doi: 10.1016/j.snb.2005.10.007.

[24] N. X. Thai, M. Tonezzer, L. Masera, H. Nguyen, N. Van Duy, and N. D. Hoa, "Multi gas sensors using one nanomaterial, temperature gradient, and machine learning algorithms for discrimination of gases and their concentration," *Anal. Chim. Acta*, vol. 1124, pp. 85–93, 2020, doi: 10.1016/j.aca.2020.05.015.

[25] V. A. Minh, L. A. Tuan, T. Q. Huy, V. N. Hung, and N. Van Quy, "Enhanced NH_3 gas sensing properties of a QCM sensor by increasing the length of vertically orientated ZnO nanorods," *Appl. Surf. Sci.*, vol. 265, pp. 458–464, 2013, doi: 10.1016/j.apsusc.2012.11.028.

[26] S. R. Systems, "QCM200 Digital Controller: Operation and Service Manual," *Oper. Serv. Man.*, vol. Revision 2, 2018.

[27] B. T. Pham *et al.*, "Development of artificial intelligence models for the prediction of Compression Coefficient of soil: An application of Monte Carlo sensitivity analysis," *Sci. Total Environ.*, vol. 679, pp. 172–184, 2019, doi: 10.1016/j.scitotenv.2019.05.061.

[28] B. Mumyakmaz, A. Özmen, M. A. Ebeoğlu, C. Taşaltin, and I. Gürol, "A study on the development of a compensation method for humidity effect in QCM sensor responses," *Sensors Actuators, B Chem.*, vol. 147, no. 1, pp. 277–282, 2010, doi: 10.1016/j.snb.2010.03.019.

[29] M. T. Hagan and M. B. Menhaj, "Training feedforward networks with the Marquardt algorithm," *IEEE Trans. Neural Networks*, vol. 5, no. 6, pp. 989–993, 1994, doi: 10.1109/72.329697.

[30] R. Kohavi, "A Study of Cross-Validation and Bootstrap for Accuracy Estimation and Model Selection," *Int. Jt. Conf. Artif. Intell.*, no. June, 1995.

[31] Y. Jung and J. Hu, "A K-fold averaging cross-validation procedure," *J. Nonparametr. Stat.*, vol. 27, no. 2, pp. 167–179, 2015, doi: 10.1080/10485252.2015.1010532.

[32] S. Saud, B. Jamil, Y. Upadhyay, and K. Irshad, "Performance improvement of empirical models for estimation of global solar radiation in India: A k-fold cross-validation approach," *Sustain. Energy Technol. Assessments*, vol. 40, no. April, p. 100768, 2020, doi: 10.1016/j.seta.2020.100768.

[33] J. Lee Rodgers and W. A. Nicewander, "Thirteen Ways to Look at the Correlation Coefficient," *Am. Stat.*, vol. 42, no. 1, pp. 59–66, Feb. 1988, doi: 10.1080/00031305.1988.10475524.

[34] S. H. Dewi and W. A. Adi, "Synthesis and characterization of high purity Fe_3O_4 and α-Fe_2O_3 from local iron sand," *J. Phys. Conf. Ser.*, vol. 1091, no. 1, p. 012021, Sep. 2018, doi: 10.1088/1742-6596/1091/1/012021.

[35] M. I. Dar and S. A. Shivashankar, "Single crystalline magnetite, maghemite, and hematite nanoparticles with rich coercivity," *RSC Adv.*, vol. 4, no. 8, pp. 4105–4113, 2014, doi: 10.1039/c3ra45457f.

[36] E. HERRERO, "Influence of synthesis conditions on the γ-Fe_2O_3 properties," *Solid State Ionics*, vol. 101–103, pp. 213–219, Nov. 1997, doi: 10.1016/S0167-2738(97)84033-7.

[37] G. Sauerbrey, "Verwendung von Schwingquarzen zur W ~ igung diinner Schichten und zur Mikrow ~ igung *," vol. 222, pp. 206–207, 1959.